Ion conduction across nanosized CaF_2/BaF_2 multilayer heterostructures

X. X. Guo,[a),b)] I. Matei, J.-S. Lee,[c)] and J. Maier[a),d)]
Max-Planck-Institut für Festkörperforschung, Heisenbergstr. 1, D-70569 Stuttgart, Germany

(Received 28 June 2007; accepted 13 August 2007; published online 4 September 2007)

The authors investigate the ion conduction of molecular beam epitaxy grown CaF_2/BaF_2 multilayers *perpendicular* to the interfaces. Unlike previous measurements along the heterostructure boundaries, the more resistive contributions dominate here; the detailed analysis allows for a complementary insight into the charge carrier distribution. The features of perpendicular conductivites in both semi-infinite and mesoscopic situations can be qualitatively as well as quantitatively explained by the same defect chemical model used for parallel ion conduction. The authors can distinguish three different size regimes. For large interfacial spacings ($\ell > 50$ nm), the conduction is dominated by bulk parts of the CaF_2 layers, showing only a slight increase with decreasing layer thickness. For very small spacings, i.e., $\ell < 30$ nm, the conductivity increases steeply and tends toward a saturation value, corresponding to the space charge overlap situation with the overall value that can be attributed to F_i' accumulated in CaF_2. The intermediate range ($30\ \text{nm} < \ell < 50$ nm) is characterized by markedly lower activation energies in which the transition from F_i' (depleted near the interface) to $V_F^{\bullet}$ (enriched near the interface) in BaF_2 plays a significant role. © *2007 American Institute of Physics*. [DOI: 10.1063/1.2779254]

Electrochemical devices associated with ion transport are complementing electronic devices. They enable the transformation of chemical information and energy into electrical information and energy, as verified in chemical sensors, batteries, and fuel cells.[1–3] Similar to electronic transport which can be tuned by varying the interfacial spacing,[4–7] ionic conduction of solid electrolytes can also be manipulated by such interfacial design.[8–16] Not only strong variations in conductivity can be achieved but also qualitative effects such as changing the type of conductivity can be observed.[8,10,15]

The significance of interfacial effects have been strikingly demonstrated by molecular beam epitaxy (MBE)-grown CaF_2/BaF_2 multilayer heterostructures.[16,17] In the direction parallel to the interfaces, the ionic conductivity was shown to increase with decreasing interface spacing (ℓ). For very thin layers in which the boundary zones overlap, an artificial ionic conductor with mesoscopic ion conduction is generated. These features have been recently quantitatively interpreted by space charge calculations based on a Mott-Schottky model with the assumption of frozen-in impurity profiles.[18] Figure 1 gives a typical concentration distribution of point defects at such a contact (500 K): fluoride interstitials (F_i') in BaF_2 as majority carriers compensated by positive dopants in the bulk are depleted and fluoride vacancies ($V_F^{\bullet}$) as minority carriers are enriched in the space charge zone. As a consequence of total electroneutrality, F_i' in CaF_2 are therefore significantly increased while the $V_F^{\bullet}$ carriers are depleted. The effective width of the space charge region ($2\lambda^*$) in BaF_2 is about 40 nm while it is much narrower in CaF_2 (Gouy-Chapman layer). The mechanism therein refers to a transfer of fluoride ion from BaF_2 to CaF_2 in the respective space charge regions, leading to an equality of the electrochemical potential of F_i'. While the more conductive parts predominate conduction along the interfaces of CaF_2/BaF_2 heterolayers, the more resistive parts must play a decisive role for the transport perpendicular to the interfaces. Therefore, perpendicular measurements can provide useful complementary information as to the charge carrier distribution.

Heterostructures composed of alternating CaF_2/BaF_2 thin layers with individual thicknesses ranging from 6 to 200 nm were deposited by MBE on 1.0 wt % Nb-doped $SrTiO_3$(100) (STO:Nb) substrates, which exhibited negligible resistances during measurement. The growth conditions are the same as for previous reports.[16,17,19] Also similar to the previous parallel investigations, BaF_2 was deposited first and the layers (both BaF_2 and CaF_2) had exclusively [111]

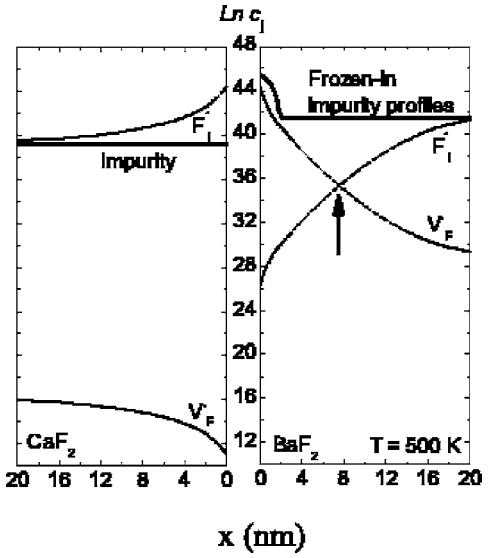

FIG. 1. Defect concentration profiles at $T = 500$ K for semi-infinite CaF_2/BaF_2 layers developed on the results of the parallel conductivities (Ref. 18). Mott-Schottky profiles with frozen-in impurity are shown for BaF_2, while Gouy-Chapman profiles for CaF_2.

[a)]Authors to whom correspondence should be addressed.
[b)]FAX: +49 711-689-1722; electronic mail: xiangxin.guo@fkf.mpg.de
[c)]Present address: Chonnam National University, Gwangju 500-757, Korea.
[d)]FAX: +49 711-689-1722; electronic mail: s.weiglein@fkf.mpg.de

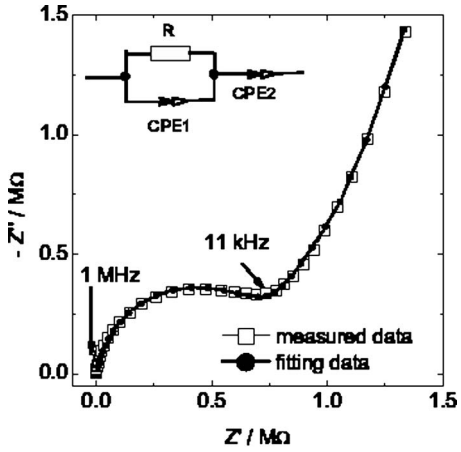

FIG. 2. Typical impedance spectrum obtained during perpendicular measurement of heterolayers. The equivalent circuit used for fitting the experimental data is shown in the inset.

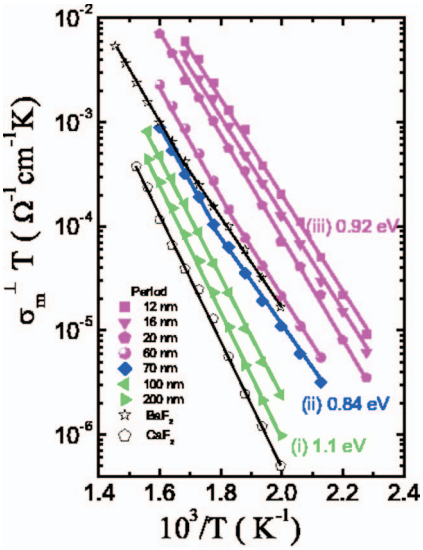

FIG. 3. (Color) Perpendicular ionic conductivity of the heterolayers with various periods ranging from 12 to 200 nm compared to the CaF_2 and BaF_2 films of 400-nm-thick. The overall thickness is approximately the same for all the samples (~400 nm). The different colors refer to different size regimes.

orientation. Smooth and continuous heterolayers with an individual layer thickness as thin as 6 nm were achieved.

For conductivity measurements, microelectrodes of Cr/Au of 100 μm in diameter with distances of 500 μm were evaporated on the sample surfaces serving as top electrodes. The bottom side of the sample was covered by Cr/Au and then attached to a metal plate (counterelectrode) by a conducting Ag paste. An Ir/Pt probe tip mounted on a micromanipulator connected to a Novocontrol Alpha-A analyzer was used for impedance spectroscopy. The measurements were carried out in argon atmosphere at frequencies ranging from 1 to 2 MHz as the temperature decreases from 690 to 435 K. A typical spectrum is shown in Fig. 2, which is characterized by a partial semicircle with a large tail resulting from the polarization effects by the blocking electrodes. Using the equivalent circuit shown in the inset of Fig. 2 an effective resistance (R) and a capacitance (C) can be extracted from the partial semicircle. According to $C=\varepsilon_0\varepsilon A/L=\varepsilon_0\varepsilon\pi(D/2)^2/L$ (where ε_0 and ε are the relative permittivity and the dielectric constant of measured sample, respectively, L the total thickness, and D the diameter of microelectrode), the calculated ε is approximately equal to 7.0, which is close to the theoretical values for CaF_2 (~6.7) and BaF_2 (~7.2).[20] Hence, the semicircle arises from the heterolayers and the overall perpendicular conductivity ($\sigma_m^{\perp}$) can be obtained by $\sigma_m^{\perp}\cong(1/R)[L/\pi(D/2)^2]$.

Measured conductivities for samples with varied periods (12~200 nm) are shown in Fig. 3. Here, the period refers to one pair of BaF_2 and CaF_2 which have the same thickness value. As regards the activation energies (E_a), the progressive increase of the measured conductivities with decreasing layer thickness (ℓ) exhibits three regimes: (i) For $\ell>50$ nm, the samples behave similarly to the 400-nm-thick CaF_2 films with an $E_a\sim1.1$ eV. (ii) For 30 nm$<\ell<$50 nm, the plot shows a lower activation energy, especially in the low T range where $E_a\sim0.84$ eV. (iii) For $\ell<30$ nm, the conductivities increase significantly with an $E_a\sim0.92$ eV.

On a qualitative level, regimes (i) and (iii) can be directly understood according to the defect profiles shown in Fig. 1. Heterolayers with $\ell>50$ nm are in a semi-infinite situation. In contrast with the parallel conductance, now the influence of interfaces is smaller than that of the more resistive bulk (σ_∞). As $\sigma_\infty(CaF_2)<\sigma_\infty(BaF_2)$,[21,22] the activation energy corresponds to that of CaF_2 bulk. For $\ell<30$ nm, the space charge regions significantly overlap. All carriers are in a close-to-interface situation, of which again the CaF_2 part is the more resistive. The mobility value of F_i' is around two orders of magnitude smaller than that of $V_F^{\bullet}$ in the temperature range of consideration. As a result, the enriched F_i' determine the overall conduction. This is consistent with the observed value of $E_a\sim0.92$ eV, which is close to the migration enthalpy of F_i' in CaF_2 (0.93 eV).[22]

As for the intermediated regime (30 nm$<\ell<$50 nm), the predicted conductivity behavior is in line with our results, as indicated by the following quantitative analysis. It is important to notice that it is the region around the minimum (referred to the intersection between $V_F^{\bullet}$ and F_i' concentration profiles, see also the arrow in Fig. 1) in BaF_2 that now becomes decisive (note that this minimum will shift to a larger thickness value if conductivity taken into account because the mobility of F_i' is much smaller than that of $V_F^{\bullet}$ (Ref. 21)). In more precise terms, it is the decrease in F_i' that makes this region more resistive than CaF_2 as long as the increase in $V_F^{\bullet}$ does not predominate.

The inverse average perpendicular conductivity (representing the sample resistance) of an individual layer can be expressed as[23]

$$(\sigma_m^{\perp})^{-1}=\phi_{sc}(\sigma_{sc}^{\perp})^{-1}+(1-\phi_{sc})(\sigma_{\infty}^{\perp})^{-1}, \quad (1)$$

where ϕ_{sc}, $\sigma_{sc}^{\perp}$, and $\sigma_{\infty}^{\perp}$ are the proportion of space charge region, (mean) perpendicular conductivities of space charge layer, and bulk, respectively. Obviously, $\phi_{sc}=2\lambda^*/\ell$ and $\sigma_{\infty}^{\perp}=ec_{V_F^{\bullet},\infty}\mu_{V_F^{\bullet}}+ec_{F_i',\infty}\mu_{F_i'}$ (where e, c_∞, and μ are the absolute value of the electronic charge, carrier concentration in bulk, and carrier mobility, respectively). $\sigma_{sc}^{\perp}$ can be obtained by[2]

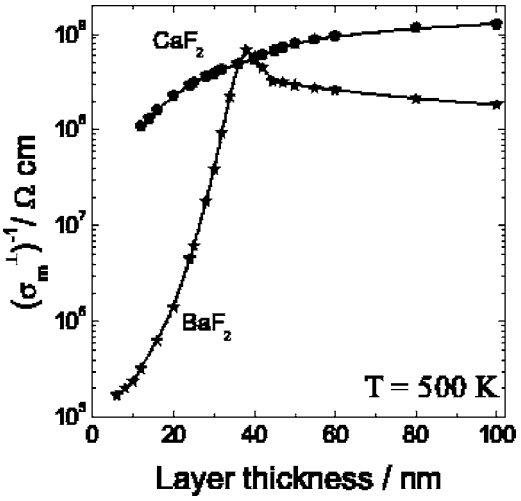

FIG. 4. Calculated inverse perpendicular conductivities $(\sigma_m^{\perp})^{-1}$ as a function of thickness (ℓ) for individual layers of CaF_2 and BaF_2 in heterolayers at 500 K. For 30 nm $<\ell<$50 nm, the values of BaF_2 are close to those of CaF_2.

$$(\sigma_{\mathrm{sc}}^{\perp})^{-1} = \frac{1}{\ell_{\mathrm{sc}}}\int_0^{\ell_{\mathrm{sc}}} \frac{1}{\sigma_{\mathrm{sc}}(x)}dx$$

$$= \frac{1}{\ell_{\mathrm{sc}}}\int_0^{\ell_{\mathrm{sc}}} \frac{1}{e\mu_{V_{\mathrm{F}}^{\bullet}}c_{\mathrm{sc},V_{\mathrm{F}}^{\bullet}}(x) + e\mu_{\mathrm{F}_i'}c_{\mathrm{sc},\mathrm{F}_i'}(x)}dx. \qquad (2)$$

According to Eq. (2), numerical calculations based on carrier concentration profiles have been performed for both CaF_2 and BaF_2 at 500 K. The results are shown in Fig. 4. Thermodynamic data are from Refs. 21 and 22. Three regimes can also be clearly distinguished. In particular, for $30<\ell<50$ nm, we observe the effect of the conductivity minimum in BaF_2 (see Fig. 1). $(\sigma_m^{\perp})^{-1}$ values of BaF_2 increase and at lower temperatures become comparable to those of CaF_2. Now F_i' in both materials dominate the overall conduction. These results are in good agreement with the observed $E_a \sim 0.84$ eV in the lower temperature range, which is in between the migration enthalpy of F_i' in CaF_2 (0.92 eV) and in BaF_2 (0.79 eV).[21,22]

In summary, we have succeeded in measuring conductivities perpendicular to interfaces of MBE-grown CaF_2/BaF_2 multilayer heterostructures by using conductive Nb-doped $SrTiO_3$ substrates. The detailed analysis points toward the following: in the semi-infinite situation $(\ell>50$ nm), the bulk parts of CaF_2 layers are the dominant factors due to their more resistive contribution. At the initial overlap situation $(30\ \mathrm{nm}<\ell<50\ \mathrm{nm})$, defect distributions with Mott-Schottky profiles lead to conductivities of CaF_2 comparable to those of BaF_2, characterized by interplay of two carriers, i.e., F_i' in CaF_2 and F_i' in BaF_2. In the strong overlap situation $(\ell<30$ nm), enriched F_i' carriers in CaF_2 dominate the conductivities. A good agreement is obtained between the experimental data and the theoretical calculation. Complementary to parallel conduction, the mesoscopic ion conduction and the details of the defect chemical description[18] have been independently corroborated by the perpendicular measurements performed here.

The authors thank Y.-G. Guo and J. Jamnik for many helpful discussions, and G. Gregori for critical reading of the manuscript.

[1] T. Kudo and K. Fueki, *Solid State Ionics* (Kodansha, Tokyo, 1990), p. 157.
[2] J. Maier, *Physical Chemistry of Ionic Materials Ions and Electrons in Solids* (Wiley, Chichester, 2004), pp. 230 and 399.
[3] J. Maier, Nat. Mater. **4**, 805 (2005).
[4] S. M. Sze, *Semiconductor Devices* (Wiley, New York, 1985).
[5] L. E. Brus, J. Chem. Phys. **80**, 4403 (1984).
[6] K. Ploog, *Springer Proceedings in Physics 22*, edited by G. L. Derrien, J. Derrien, and N. Boccara (Springer, Berlin, 1987), pp. 10–42.
[7] R. J. Haug, M. Diler, T. Schmidt, R. H. Blick, K. von Klitzing, and K. Eberl, Physica B **227**, 82 (1996).
[8] S. Kim and J. Maier, J. Electrochem. Soc. **149**, J73 (2002).
[9] P. Balaya, J. Jamnik, J. Fleig, and J. Maier, Appl. Phys. Lett. **88**, 062109 (2006).
[10] Y.-M. Chiang, E. B. Lavik, I. Kosacki, H. L. Tuller, and J. Y. Ying, Appl. Phys. Lett. **69**, 185 (1996).
[11] H. L. Tuller, Solid State Ionics **131**, 143 (2000).
[12] X. Guo, C. Pithan, C. Ohly, C.-L. Jia, J. Dornseiffer, F.-H. Haegel, and R. Waser, Appl. Phys. Lett. **86**, 082110 (2005).
[13] S. Azad, O. A. Marina, C. M. Wang, L. Saraf, V. Shutthanandan, D. E. McCready, A. El-Azab, J. E. Jaffe, M. H. Engelhard, C. H. F. Peden, and S. Thevuthasan, Appl. Phys. Lett. **86**, 131906 (2005).
[14] A. Peters, C. Korte, D. Hesse, N. Zakharov, and J. Janek, Solid State Ionics **178**, 67 (2007).
[15] J. Maier and B. Reichert, Ber. Bunsenges. Phys. Chem. **90**, 666 (1986).
[16] N. Sata, K. Eberl, K. Eberman, and J. Maier, Nature (London) **408**, 946 (2000).
[17] X. X. Guo, N. Sata, and J. Maier, Electrochim. Acta **49**, 1091 (2004).
[18] X. X. Guo, I. Matei, J. Jamnik, J. S. Lee, and J. Maier, Phys. Rev. B (to be published).
[19] X. X. Guo and J. Maier, Surf. Sci. **549**, 211 (2004).
[20] W. Kaiser, W. G. Spitzer, R. H. Kaiser, and L. E. Howarth, Phys. Rev. **127**, 1950 (1962).
[21] E. Barsis and A. Taylor, J. Chem. Phys. **48**, 4357 (1968); **48**, 4362 (1968).
[22] W. Bollmann and H. Henniger, Phys. Status Solidi A **11**, 367 (1972); **16**, 187 (1973).
[23] J. Maier, Ber. Bunsenges. Phys. Chem. **90**, 26 (1986).